Biomacromolecules

pubs.acs.org/Biomac

Article

Construction and Piezoelectric Properties of a Single-Peptide Nanotube Composed of Cyclic β-peptides with Helical Peptides on the Side Chains

Taichi Kurita, Tomoaki Terabayashi, Shunsaku Kimura, Keiji Numata,* and Hirotaka Uji*

Cite This: *Biomacromolecules* 2021, 22, 2815−2821

Read Online

ACCESS | Metrics & More | Article Recommendations | Supporting Information

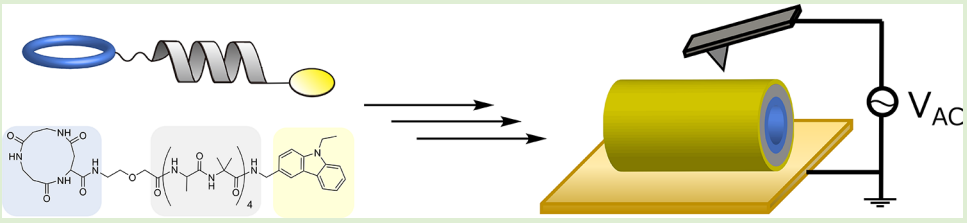

ABSTRACT: To develop nanopiezoelectronics, it is necessary to investigate the relationship between the sizes and piezoelectric properties of the material. Peptide nanotubes (PNTs) composed of cyclic β-peptides have been studied as leading candidates for nanopiezoelectric materials. The current drawback of PNTs is aggregation to form a PNT bundle structure due to strong dipole−dipole interactions between PNTs. Here, we report the construction and piezoelectric properties of single PNTs without nonspecific aggregation by side-chain modification of helical peptides. A cyclic tri-β-peptide with a helical peptide was prepared by multiple-step liquid-phase peptide synthesis and assembled into PNTs by the vapor diffusion method. These nanotubes were characterized by polarized light microscopy and Fourier transform infrared (FTIR) spectroscopy. Additionally, atomic force microscopy (AFM) topographic images showed nanotubes with a height of 4 nm, which corresponds to the diameter of a PNT on a gold-coated mica substrate, indicating that a single PNT was prepared successfully. The converted piezoelectric response of a single PNT was determined to be 1.39 ± 0.12 pm/V. This value was consistent with that of a PNT bundle, which reveals that the piezoelectricity of PNTs is induced by deformation of their cyclic skeletons and is independent of the bundled structure. This finding not only demonstrates a new molecular design strategy to construct these smallest piezoelectric biomaterials by controlling the supramolecular hierarchical structures but also provides insights into the correlation between molecular assembly morphology and size-dependent piezoelectric properties.

INTRODUCTION

Sensors are expected to play a crucial role in linking things to the Internet in the coming era of the Internet of Things (IoT).[1,2] Specifically, monitoring the human body is a very significant part of providing personalized and preventative healthcare and an opportunity to identify diseases at an early stage.[3] Since piezoelectric nanomaterials convert mechanical movements into electrical power, they are rational candidates for tiny sensors and the power sources of various microelectronics.[4−7] Organic piezo materials have some advantages in terms of biocompatibility, flexibility, low weight, and low production cost and have been extensively studied.[8−10] For example, nanotubes prepared from diphenylalanine (FF) and FF-based peptides have been reported as biopiezoelectric materials.[11−14] In recent years, these biocompatible piezoelectric materials have been studied for application in implantable medical electronics (IMEs), such as cardiac pacemakers, active pressure sensors, and devices for the direct stimulation of tissue and living cells.[4] Piezoelectric materials with small dimensions are highly desired for IMEs, as they have little influence on human activities and can be adapted to the curved and corrugated surfaces of human organs.[4] However, controversy over the size-dependent piezoelectricity when piezoelectric materials are decreased in size has long existed. In the case of poly(vinylidene fluoride trifluoroethylene) (PVDF) nanofibers synthesized by the electrospray method, the piezoelectricity increases upon reduction of the material size to the nanoscale.[15] In nanotubes prepared by assembling FF dipeptides, the piezoelectric coefficient decreases as the fiber diameter decreases.[11] The relationship between the size and piezoelectric properties of a material is still not fully understood, and further investigations are needed for the development of nanopiezoelectronics.

Received: February 16, 2021
Revised: April 4, 2021
Published: May 17, 2021

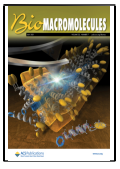

https://doi.org/10.1021/acs.biomac.1c00213
Biomacromolecules 2021, 22, 2815−2821

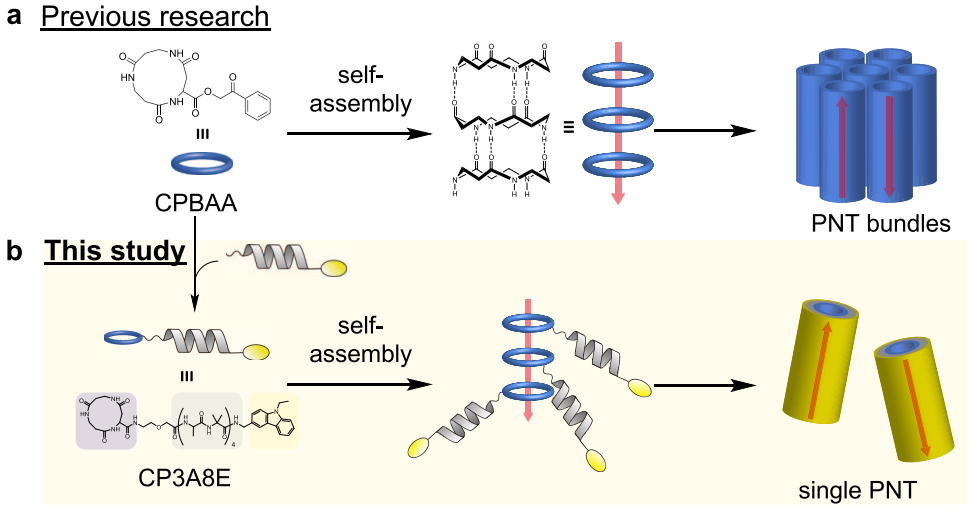

Figure 1. (a) Schematic illustration of PNT bundle formation reported in a previous study. (b) Schematic illustration of single PNT formation in this study. Each red arrow indicates the dipole moment of PNT.

Cyclic peptides composed of alternating D and L amino acids, β-amino acids, or α- and γ-amino acids have been widely reported to self-assemble into peptide nanotubes (PNTs) via intermolecular hydrogen bonds.[16−21] The advantage of PNTs constructed from cyclic peptides is that the nanotube size can be controlled depending on the number of cyclic amino acid residues, resulting in well-defined nanostructures.[22] In particular, PNTs prepared from cyclic β-peptides have been reported to have piezoelectric properties.[23−25] One disadvantage of PNTs consisting of cyclic β-peptides is that PNTs easily aggregate to form PNT bundle structures due to the large dipole moment along the nanotube axis, resulting in strong dipole−dipole interactions between PNTs (Figure 1a).[26,27] It is therefore challenging to prepare a single PNT or a bundle of PNTs with a defined number. To control the bundle size, functional moieties were introduced into the side chains of cyclic peptides by, for example, G-quartet formation[28] and side-chain polymerization.[29] α,γ-PNTs bearing fullerene side chains were also reported to form a defined bundle structure due to self-assembly of fullerene arrangements.[30] Recently, the introduction of charged side-chain moieties, such as naphthalimide (Npi) groups[31] or chloranil groups,[32] to cyclic β-peptides was found to lead to the formation of single PNTs in aqueous solutions, preventing bundle formation by electrostatic repulsion. These ionic functional groups can affect the piezoelectric properties; therefore, it is necessary to construct single PNTs with nonionic functional moieties. We focused our attention on helical peptides with a dipole moment from the C-terminus to the N-terminus, generating an electrostatic potential field.[33,34] The field of the helical peptide macrodipole is considered to be equal to the field of a positive charge at the N-terminus and a negative charge at the C-terminus, where the magnitude of each is determined to be 1/2 of the elementary charge. In addition, helical peptides adopt a three-dimensional bulky structure, which is expected to hinder close contact among PNTs. Therefore, the introduction of helical peptides into the PNT side chain is expected to effectively form single PNTs.

In this study, we designed and synthesized a cyclic tri-β-peptide (CP3A8E) that has an octapeptide with an alternating sequence of Ala and α-aminoisobutyric acid (Aib) on the side chains and that is reported to adopt a helical structure.[35,36] Using AFM measurements, we confirmed that CP3A8E was successfully self-assembled into a single PNT. The piezoresponse properties of the single PNTs were evaluated by piezoelectric force microscopy (PFM), and their size-dependent piezoelectric properties were further discussed.

EXPERIMENTAL SECTION

Materials. Chemical reagents were obtained from Tokyo Chemical Industry Co., Ltd. (Tokyo, Japan); Watanabe Chemical Industries Ltd. (Hiroshima, Japan); Fujifilm Wako Pure Chemical Industries, Ltd. (Osaka, Japan); and Oakwood Chemical (Estill, SC) and used without further purification.

Characterization Procedures. ^{1}H NMR spectra were recorded on a Bruker DPX-400 NMR spectrometer (Bruker Biospin, Rheinstetten, Germany) at 25 °C and 400 MHz. Chloroform-*d* or deuterated dimethyl sulfoxide (DMSO-d_6) was used as the NMR solvent. Electrospray ionization (ESI) mass spectrometric analysis was conducted using a Thermo Fisher Scientific Exactive Plus Orbitrap ESI mass spectrometer (Thermo Fisher Scientific, Waltham, MA). The purity of the final compounds was confirmed by reversed-phase high-performance liquid chromatography (RP-HPLC). The RP-HPLC analyses were performed on an HPLC system consisting of an autosampler SIL-20AC, a gradient pump LC-20AD, a column oven CTO-20AC, a UV/vis detector SPD-M20A (Shimadzu Corporation, Kyoto, Japan), and a Cosmosil C18-MS packed column (5 μm, 46 mm i.d. × 150 mm, Nacalai Tesque, Inc., Kyoto, Japan).

Synthesis of Boc-(Ala-Aib)$_4$-NH-CH$_2$-Ecz (1). Boc-(Ala-Aib)$_4$-OH (BA8OH) was synthesized according to previous studies.[35,36] BA8OH (490 mg, 660 μmol) and 3-*N*-ethylcarbazolylmethylamine (182.3 mg, 812 μmol) were dissolved in dry *N*,*N*-dimethylformamide (DMF, 10 mL). A mixed solution of (1-cyano-2-ethoxy-2-oxoethylidenaminooxy)dimethylamino-morpholino-carbenium hexafluorophosphate (COMU, 423 mg, 989 μmol) and ethyl (hydroxyimino)cyanoacetate (Oxyma, 141 mg, 989 μmol) in dry DMF (2 mL) and diisopropylethylamine (DIEA, 0.4 mL, 2.29 mmol) were added sequentially at 0 °C, and the reaction mixture was stirred for 18 h at 25 °C under an argon atmosphere. The solvent was removed under reduced pressure. The residue was dissolved in chloroform, and the solution was washed three times with 4 wt % $KHSO_4$ (aq.) and sat. $NaHCO_3$ (aq.). The organic layer was washed with brine, dried over anhydrous Na_2SO_4, filtered, and concentrated under reduced pressure. The residue was purified by column chromatography (silica gel, eluent: chloroform/MeOH = 10/1 v/v) to obtain compound **1** as a yellow solid. Yield: 401 mg, 422 μmol (64%).

https://doi.org/10.1021/acs.biomac.1c00213
Biomacromolecules 2021, 22, 2815−2821

^{1}H NMR (400 MHz, $CDCl_3$, δ): 1.35−1.65 (m, 48H, Boc, AlaC$^{\beta}H_3$, AibC$^{\beta}H_3$, NCH$_2$CH_3), 3.77−3.87 (m, 2H, CH_2CH$_3$), 3.87−3.95, 4.40−4.57, 4.63-4.71 (m, 4H, AlaC$^{\alpha}H$), 4.27−4.35 (m, 2H, CH_2-Ecz), 5.92 (s, 1H, urethane), 6.91−8.07 (m, 14H, carbazolyl-*H*, AlaN*H*, AibN*H*).

ESI-MS (m/z): $[M + Na]^+$ calcd for $C_{48}H_{72}N_{10}O_{10}Na$, 971.5325; found, 971.5312.

Synthesis of Boc-(2-aminoethoxy carbonyl)-(Ala-Aib)$_4$-NH-CH$_2$-Ecz (2). The Boc group of compound **1** (401 mg, 380 μmol) was deprotected by treatment with 4 N HCl/1,4-dioxane (35 mL). The reaction mixture was stirred for 1 h at 25 °C. The solvent was removed under reduced pressure, and the crude product was washed with diisopropyl ether and concentrated under reduced pressure. Deprotected compound **1** (350 mg, 395 μmol) and (2-boc-aminoethoxy)acetic acid (127 mg, 579 μmol) were dissolved in dry DMF (4 mL). A mixed solution of COMU (244 mg, 570 μmol) and Oxyma (81 mg, 570 μmol) in dry DMF (2 mL) and DIEA (0.2 mL, 1.14 mmol) were added sequentially at 0 °C, and the reaction mixture was stirred for 18 h at 25 °C under an argon atmosphere. The solvent was removed under reduced pressure. The residue was dissolved in chloroform and washed three times with 4 wt % $KHSO_4$ (aq.) and sat. $NaHCO_3$ (aq.). The organic layer was washed with brine, dried over anhydrous Na_2SO_4, filtered, and concentrated under reduced pressure. The residue was washed with diisopropyl ether three times to afford compound **2**. Yield: 297 mg, 283 μmol (74%)

^{1}H NMR (400 MHz, $CDCl_3$, δ): 1.36−1.64 (m, 48H, Boc, AlaC$^{\beta}H_3$, AibC$^{\beta}H_3$, CH$_2$CH_3), 3.59−3.69 (m, 4H, NHCH$_2$CH_2O, NHCH$_2$CH_2O) 3.82−3.90 (m, 2H, NCH_2CH$_3$), 3.95−4.02, 4.39−4.45, 4.69−4.78 (m, 4H, AlaC$^{\alpha}H$), 4.02−4.06 (m, 2H, OCH_2CO), 4.29−4.36 (m, 2H, CH_2-Ecz), 5.15 (s, 1H, urethane), 6.91−8.07 (m, 14H, carbazolyl-*H*, AlaN*H*, AibN*H*).

ESI-MS (m/z): $[M + Na]^+$ calcd for $C_{52}H_{79}N_{11}O_{12}Na$, 1072.5802; found, 1072.5794.

Synthesis of CP3A8E. The Boc group of compound **2** (50 mg, 47.6 μmol) was deprotected by treatment with 4 N HCl/1,4-dioxane (3 mL). The reaction mixture was stirred for 1 h at 25 °C. The solvent was removed under reduced pressure, and the crude product was washed with diisopropyl ether and concentrated under reduced pressure. Deprotected compound **2** (45 mg, 45.6 μmol) and cyclo[β-Asp-β-Ala-β-Ala] (10 mg, 38.9 μmol) synthesized according to the literature[32] were dissolved in dry DMF (1.5 mL). A mixed solution of *o*-(7-azobenzotriazol-1-yl)-1,1,3,3-tetramethyluronium hexafluorophosphate (HATU, 23.2 mg, 61.0 μmol) and 1-hydroxy-7-azabenzotriazole (HOAt, 11.3 mg, 83.0 μmol) in dry DMF (0.5 mL) and DIEA (30 μL, 171 μmol) were added sequentially at 0 °C, and the reaction mixture was stirred for 36 h at 25 °C under an argon atmosphere. The solvent was removed under reduced pressure. The residue was washed with acetonitrile and purified by column chromatography (Sephadex LH20, eluent: DMF) twice to afford the desired compound **CP3A8E**. Yield: 21 mg, 21 μmol (46%)

^{1}H NMR (400 MHz, $CDCl_3$, δ): 1.36−1.64 (m, 39H, AlaC$^{\beta}H_3$, AibC$^{\beta}H_3$, CH$_2$CH_3), 1.99−2.13 (m, 2H, β-AspC$^{\alpha}H$), 2.30−2.57 (m, 4H, β-AlaC$^{\alpha}H_2$), 3.09−3.53 (m, 8H, β-AlaC$^{\beta}H_2$, NHCH_2CH$_2$O, NHCH$_2$CH_2O), 3.81−3.89 (m, 2H, CH_2CH$_3$), 3.91 (s, 2H, OCH_2CO), 4.06−4.21, 4.32−4.45 (m, 4H, AlaC$^{\alpha}H$), 4.39−4.42 (d, 2H, CH_2-Ecz), 4.45−4.55 (m, 1H, β-Asp C$^{\beta}H$) 7.12−8.45 (m, 20H, carbazolyl-*H*, AlaN*H*, AibN*H*, β-AlaN*H*, β-AspN*H*).

ESI-MS (m/z): $[M + Na]^+$ calcd for $C_{57}H_{84}N_{14}O_{14}Na$, 1211.6192; found, 1211.6184.

Spectroscopic Microscopy. Circular dichroism (CD) spectra were recorded at 25 °C on a JASCO J-1500 CD spectrometer (JASCO, Tokyo, Japan). The peptide solutions at a concentration of 1.25×10^{-4} M were placed in an optical cell with a 1 cm path length to measure the CD spectra.

Vapor Diffusion Method. CP3A8E was dissolved in a good solvent (100 μL) was placed in a glass vial of 35 mm in height and 12 mm in diameter (vial A). The poor solvent (3.0 mL) was placed in another glass vial of 55 mm in height and 27 mm in diameter (vial B). Then vials A was stored in a closed vial B and left at 21 °C.

Fourier Transform Infrared (FTIR) Measurement. ATR-FTIR spectra were recorded on an IRPrestigae-21 FTIR spectrophotometer (Shimadzu Corporation, Kyoto, Japan) with a MIRacle A single reflection ATR unit using a Ge prism. The PNT dispersion was dropped on a Ge prism and dried naturally at 25 °C. The measurements were conducted from 4000 to 800 cm^{-1}. Background spectra obtained under the same conditions were subtracted from each sample spectrum.

Optical Microscopy. Optical microscopy was performed with an Olympus IX70 optical microscope (Olympus, Tokyo, Japan). The PNT dispersion was dropped on a glass substrate and dried. The peptide samples were observed between a pair of polarizing plates arranged under a cross Nicol state. The birefringence observations were performed using a sensitive tint plate.

Preparation of Gold-Mica Substrate. Gold-mica substrates for the AFM and PFM measurements were prepared by the vapor deposition method. The gold layer (99.99%, 1000 Å) was vapor-deposited onto a mica substrate by an Osaka Vacuum N-KS350 vacuum deposition system (Osaka Vacuum, Osaka, Japan). The gold-mica substrates were thermally annealed before use.

AFM and PFM Measurements. AFM measurements were carried out by means of a Bruker Multimode 8 AFM (Bruker, Santa Barbara, CA) in Peak Force QNM mode with a Bruker cantilever (SCANASYST-AIR, Al reflective coating, 0.4 N/m, 70 kHz, and SCANASYST-AIR-HR, Al reflective coating, 0.4 N/m, 130 kHz) at 25 °C under ambient atmosphere. In this study, QNM mode was used only for getting the topographic images to clear the position of the samples on the gold substrate. Ethyl acetate (5 μL) was added to the PNT dispersion (5 μL) followed by 10 s sonication treatment. This solution (5 μL) was dropped on a gold-mica substrate and dried naturally at 25 °C. This sample was subjected to both AFM and PFM measurements. PFM measurements were conducted with a Bruker cantilever (MESP-RC-V2, Co/Cr, 5.0 N/m, 150 kHz), which is recommended for the PFM measurements by Bruker. For all PFM measurements, deflection sensitivity was calibrated for every tip against a clean silicon wafer. PFM measurements were conducted at 12 different points of the sample.

RESULTS AND DISCUSSION

Secondary Structure of CP3A8E. A cyclic tri-β-peptide conjugated with a helical peptide (CP3A8E) was synthesized by means of the conventional liquid-phase method (Scheme S1), which was confirmed by HPLC, ^{1}H NMR, and ESI mass spectrometry (Figures S1−S3). The secondary structure of CP3A8E was analyzed by CD measurements in an ethanol solution (Figure 2). A negative Cotton effect at 206 nm and an adjacent broad shoulder at approximately 220 nm were observed. Based on the R ratio ($\theta_{222}/\theta_{207}$) calculated from the CD spectrum of CP3A8E (R = 0.52), the conformation of the side-chain peptide of CP3A8E was considered to be a mixture of 3_{10}- and α-helices.[37]

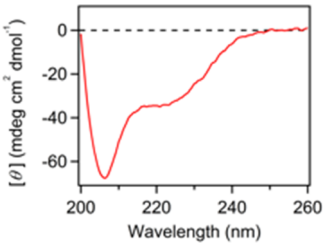

Figure 2. CD spectrum of CP3A8E in ethanol at a concentration of 0.125 mM. The corresponding HT data of the CD spectrum is given in Supporting Information (Figure S4).

Peptide Nanotube Formations. To obtain piezoelectric nanomaterials, we attempted to prepare PNTs through self-

https://doi.org/10.1021/acs.biomac.1c00213
Biomacromolecules 2021, 22, 2815−2821

assembly of CP3A8E using the vapor diffusion method, where the peptide solution in a good solvent was exposed to a poor-solvent-saturated atmosphere (Figure S5a). First, we studied the combination of good and poor solvents. Polarized microscopy under a cross Nicol configuration showed that rod-shaped crystals were obtained only when ethanol was used as the good solvent and ethyl acetate was used as the poor solvent (Figure S5). In the other solvent system, PNTs were not obtained since CP3A8E aggregated or did not form the assembly. Next, we studied the concentration of the CP3A8E solution and the incubation time under the condition that ethanol was used as the good solvent and ethyl acetate was used as the poor solvent. The CP3A8E solution was almost saturated at a concentration of 2 g/L. Polarized microscopy showed that the higher the concentration of CP3A8E was, the more crystals grew up to 24 h and after 24 h, the crystals did not grow significantly. (Figure S5). In the following experiment, CP3A8E self-assembled into PNTs under the optimized condition that 2 g/L peptide solution in ethanol was exposed to an ethyl acetate-saturated atmosphere for 24 h. Hydrogen-bond formation was confirmed by FTIR spectroscopy (Figure 3). The FTIR spectrum showed amide I, II, and N−H

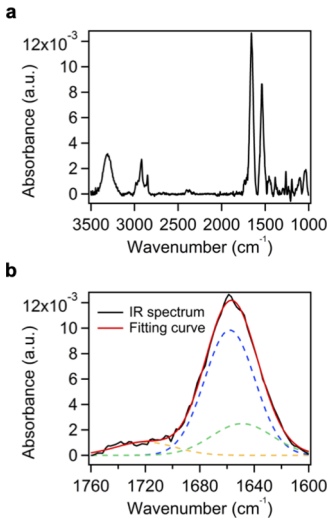

Figure 3. (a) ATR-FTIR spectrum of CP3A8E PNTs. (b) Peak separations of IR spectra in the amide I region using Gaussian functions. The red line is the fitting curve, and the broken lines represent the separate amide I peaks.

stretching peaks at 1658, 1541, and 3300 cm^{-1}, respectively. The amide I region was deconvoluted into two bands (1658 and 1649 cm^{-1}) by curve fitting. The former peak indicates the helical structure of the side-chain peptide,[38] and the latter peak indicates parallel β-sheet-type hydrogen bonds[39] similar to the PNTs reported in previous studies,[40] indicating that the PNT formed via hydrogen-bond formation of cyclic skeletons.

The molecular-assembled structure was studied by microscopy. Rod-shaped crystals approximately 40 μm in length and several micrometers in diameter were observed by polarized microscopy under a cross Nicol configuration (Figure 4a). With a sensitive tint plate, the crystals showed yellow/orange color (subtraction retardation) in the parallel direction between the long axis of the crystals and the z' axis of the tint plate and blue color (addition retardation) in the vertical direction (Figure 4b). These results suggest that the higher refractive index of the short axis is attributed mainly to the amide groups in the helical peptide and that the lower refractive index of the long axis is attributed to the stacked amide bonds of the cyclic skeleton based on the molecular polarizability analysis (Figure 4c,d).[41] Therefore, the cyclic peptides stacked against each other via hydrogen bonds to form a columnar structure, as expected from our previous studies.[40,42]

The PNT morphology of CP3A8E was studied by AFM measurements. The PNT samples for AFM measurements were obtained by dispersing the PNT crystals in ethyl acetate followed by 10 s sonication treatment. Figure 5a shows tube structures of a few micrometers in length and a thickness of 4 nm, as shown in the histogram (Figure 5c), corresponding to the diameter of CP3A8E, indicating that a single PNT was successfully obtained without bundle formation on a gold-mica substrate. Previously, we demonstrated the formation of pH-responsive bundles and single PNTs repeatedly in aqueous solution, where the charged groups introduced at the side chain cause electrostatic repulsion between the PNTs and prevent bundling.[31] Therefore, in this study, it can be presumed that the partial charge of the helical peptide at the C-terminus decreases the dipole−dipole interaction between the PNTs, causing the PNT crystals to disassemble into a single PNT during sonication treatment.

Piezoelectricity of Single PNTs. The piezoelectric properties of the single PNTs were evaluated by PFM measurements, where the conducting probe tip was placed on the surface of the single PNTs and an ac voltage was applied between the tip and gold-mica substrate. The piezoelectric response was recorded at an applied bias voltage ranging from 0 to 3 V at the cantilever. The converse piezoelectric coefficient d_{33}* value of the single PNTs was evaluated to be 1.39 ± 0.12 pm/V. This value, however, was almost the same as the d_{33}* value of 1.34 ± 0.16 pm/V for bundled PNTs, which consisted of the same cyclic peptide, cyclo[β-Asp(OBzl)-β-Ala-β-Ala] (CPBAA) and differed only in the side chain (Table 1).[24] For comparison, the d_{33}* value was evaluated for a gold-mica substrate only (Table S1). There are several factors to be considered in this piezoelectric response. The first factor is the difference in the dipole moment of the side-chain moieties. Previously, it was reported that there is no difference in piezoelectricity between PNTs with and without a benzyl ester group on the side chain.[24] Furthermore, it has also been confirmed that charge transfer complexation at the side chain of PNTs does not lead to a strong piezoelectric response but results in large surface potentials on a gold substrate.[32] Therefore, these studies indicate that in the case of PNTs, the dipole moment introduced onto the side chain has a negligible effect on the piezoelectric properties.

The second factor is the size-dependent physical properties. The size dependence of piezoelectricity has been reported in two examples (PVDF and FF dipeptide nanotubes). Here, we discuss the size dependence of piezoelectricity by comparing previous reports with our current results.[11,15] Ico et al. reported that the piezoelectric response of PVDF nanofibers was enhanced during dimension reduction and could be explained by flexoelectricity.[15] Flexoelectricity is a well-known phenomenon in which a nanomaterial consisting of fewer than dozens of molecular layers induces a larger strain gradient than a bulk material when the same surface stress is applied, which results in enhancement of the piezoelectric response or leads to piezoelectric-like properties.[43,44] PVDF nanofibers prepared by

https://doi.org/10.1021/acs.biomac.1c00213
Biomacromolecules 2021, 22, 2815−2821

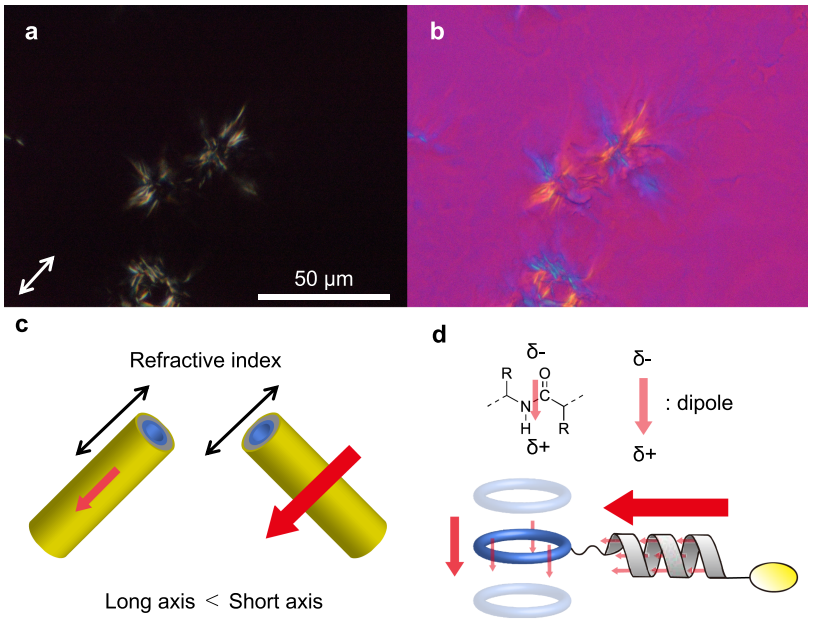

Figure 4. Optical microscopy observation of CP3A8E crystals without (a) and with (b) a sensitive tint plate in a cross Nicol arrangement. The double-headed arrow (a) shows the direction of the z'-axis of a sensitive tint plate. The scale bar is 50 μm. (c) Schematic illustration of the anisotropic refraction of CP3A8E PNTs. (d) Schematic illustration of the molecular polarity of CP3A8E PNTs. Each red arrow indicates the dipole moment of PNT.

the electrospinning procedure have a core structure and a thin sheath layer on the surface due to nonuniform evaporation of the solvent. This sheath layer remains at a constant thickness regardless of the diameter of the fiber. Therefore, it has been concluded that the increasing contribution of the sheath layer during the fiber diameter reduction induces a large strain gradient and polarization under mechanical loading, resulting in the enhanced piezoelectricity of PVDF nanofibers. On the other hand, in the case of FF dipeptide nanotubes, the piezoelectric coefficient has been reported to decrease as the diameter of FF nanotubes decreases.[11] FF dipeptide nanotubes, however, have a hollow structure due to the morphological transition from a hexagonal packing sheet to a rolled-up nanotube during self-assembly.[45,46] The inner diameter is considered to be constant, and the thickness of the nanotube is expected to increase as the number of constituent molecules increases. Thus, the thickness of the thin layer can be qualitatively explained by the piezoelectric properties of FF dipeptide nanotubes. Therefore, this hollow structure leads to a vivid contrast between FF dipeptide nanotubes and PVDF nanofibers.

The piezoelectric response of the PNTs composed of cyclic peptides reported herein was not dependent on the PNT bundle size, and the profile disagrees with the size dependencies of both PVDF and FF dipeptide nanotubes. It can be presumed that these size-dependent piezoelectric properties are attributed to differences in the assembling structure. PNT bundles are formed upon the aggregation of PNTs, and the sizes of the PNT bundles correspond to the thickness of the bundle structure, which is determined by the number of PNTs in the bundle. Regarding hierarchical morphologies, FF dipeptide nanotubes have one higher-order assembling structure than the present PNT bundles, where stacked FF hexamers form a honeycomb-like array sheet structure and then roll up to form a nanotube with a relatively large hollow structure. Furthermore, the number of cyclic peptide molecules per layer remains constant in comparison to FF dipeptide nanotubes. On the other hand, the structure of PVDF is similar to that of the PNT bundles because polymer chains are assembled into fibrils, just as supramolecular chains of PNTs are assembled into bundles in PNT bundles. In PVDF, the polymer chains aggregate heterogeneously, inducing flexoelectricity, whereas in PNT bundles, the PNTs are regularly aligned to form a lattice structure, as shown by the electron diffraction pattern, indicating a homogeneous structure without a sheath layer.[47]

Other possible factors affecting the piezoelectricity of PNT bundles composed of cyclic-β-peptides are the deformation of the cyclic peptide backbone and the interaction between PNTs. The piezoelectricity values of single PNTs and bundled PNTs were almost the same, suggesting that the piezoelectricity of the bundled PNTs originates from the deformation of the PNTs themselves, including changes in the dipole orientation of the ring skeleton upon application of an electric field, rather than from the change in structure of the bundled PNTs. In other words, the piezoelectric properties of PNTs do not change when PNTs are decreased in size as single PNTs are constructed. Considering that a single PNT with a size of 4 nm is the smallest biomaterial-based piezoelectric material, PNTs composed of cyclic peptides are promising candidates for energy harvesters in biomedical applications in microenvironments that have not been accomplished until now.

CONCLUSIONS

We have demonstrated single PNTs by introducing a helical peptide into a cyclic tripeptide. AFM images showed very thin fibril-like structures with lengths of a few micrometers and a thickness of 4 nm, which corresponds to the diameter of the PNTs, indicating that single PNTs were successfully constructed on a gold-coated mica substrate. The piezoelectricity of a single PNT was almost the same as that of a

https://doi.org/10.1021/acs.biomac.1c00213
Biomacromolecules 2021, 22, 2815−2821

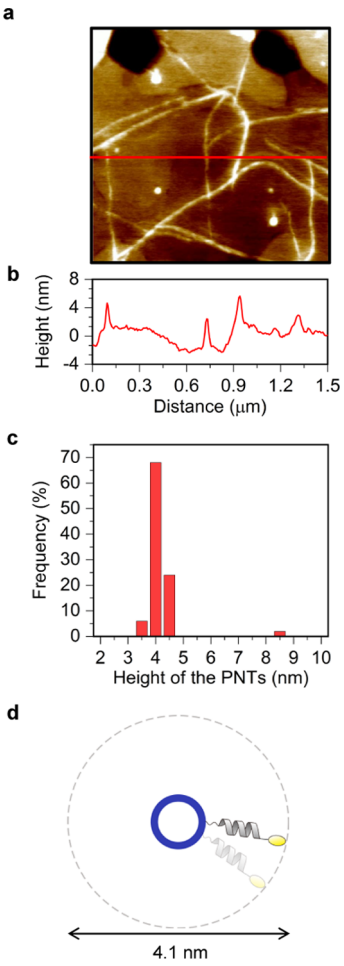

Figure 5. (a) AFM image of CP3A8E PNTs on a gold-mica substrate. (b) Height profiles along the red line in the AFM image in (a). (c) Statistical analysis of the height of the PNTs by a histogram. (d) Schematic illustration of the diameter of CP3A8E PNTs.

Table 1. Average d_{33}* Values and Standard Deviations of the Single PNTs (CP3A8E) and PNT Bundles (CP3BAA)

peptide	piezoelectric coefficient (d_{33}*) (pm/V)
CP3A8E (single PNTs)	1.39 ± 0.12
CPBAA (bundle PNTs)	1.34 ± 0.16

PNT bundle, which reveals that the piezoelectricity of the bundled PNTs was induced by their deformation behavior, not by the structural change upon bundle formation. The present study reports the piezoelectric properties of cyclic molecules. The current findings suggest a new molecular design for piezoelectric nanomaterials. Further studies of piezoelectricity upon changing the amino acids composing the cyclic peptides and controlling the size of PNT bundles by assembling an arbitrary number of PNTs will lead to next-generation piezoelectric nanomaterials.

■ ASSOCIATED CONTENT

Supporting Information

The Supporting Information is available free of charge at https://pubs.acs.org/doi/10.1021/acs.biomac.1c00213.

Scheme of the chemical synthesis of CP3A8E; ^{1}H NMR spectrum of CP3A8E; ESI MS spectrum of CP3A8E; HPLC chromatograms of CP3A8E; HT data of the CD spectrum of CP3A8E; schematic illustration and results of the vapor diffusion method; and average d_{33}* values of the single PNTs (CP3A8E) and gold-mica substrate (PDF)

■ AUTHOR INFORMATION

Corresponding Authors

Keiji Numata − *Department of Material Chemistry, Graduate School of Engineering, Kyoto University, Kyoto 615-8510, Japan; Biomacromolecules Research Team, RIKEN Center for Sustainable Resource Science, Wako, Saitama 351-0198, Japan;* orcid.org/0000-0003-2199-7420; Email: numata.keiji.3n@kyoto-u.ac.jp

Hirotaka Uji − *Department of Material Chemistry, Graduate School of Engineering, Kyoto University, Kyoto 615-8510, Japan;* orcid.org/0000-0003-0447-8944; Email: hirotaka.uji.3w@kyoto-u.ac.jp

Authors

Taichi Kurita − *Department of Material Chemistry, Graduate School of Engineering, Kyoto University, Kyoto 615-8510, Japan*

Tomoaki Terabayashi − *Department of Material Chemistry, Graduate School of Engineering, Kyoto University, Kyoto 615-8510, Japan*

Shunsaku Kimura − *Department of Material Chemistry, Graduate School of Engineering, Kyoto University, Kyoto 615-8510, Japan*

Complete contact information is available at: https://pubs.acs.org/10.1021/acs.biomac.1c00213

Author Contributions

S.K., K.N., and H.U. conceived and designed the research. T.K., H.U., and K.N. wrote the manuscript. T.K. and T.T. performed all of the experiments and analyzed the data.

Notes

The authors declare no competing financial interest.

■ ACKNOWLEDGMENTS

This research was supported partially by JSPS KAKENHI Grant No. JP19K15375 (H.U.), The Kyoto University Foundation, Iketani Science and Technology Foundation (0311024-A), JST ERATO Grant No. JPMJER1602, Japan (K.N.), Grant-in-Aid for Transformative Research Areas (B) (K.N.), and The Kyoto Technoscience Center.

■ REFERENCES

(1) Atzori, L.; Iera, A.; Morabito, G. The Internet of Things: A survey. *Comput. Networks* **2010**, *54*, 2787−2805.

(2) Bogue, R. Towards the trillion sensors market. *Sens. Rev.* **2014**, *34*, 137−142.

(3) Ciuti, G.; Ricotti, L.; Menciassi, A.; Dario, P. MEMS sensor technologies for human centred applications in healthcare, physical activities, safety and environmental sensing: a review on research activities in Italy. *Sensors* **2015**, *15*, 6441−6468.

(4) Ali, F.; Raza, W.; Li, X.; Gul, H.; Kim, K.-H. Piezoelectric energy harvesters for biomedical applications. *Nano Energy* **2019**, *57*, 879−902.

(5) Ghosh, S. K.; Mandal, D. High-performance bio-piezoelectric nanogenerator made with fish scale. *Appl. Phys. Lett.* **2016**, *109*, No. 103701.

(6) Guerin, S.; Tofail, S. A. M.; Thompson, D. Organic piezoelectric materials: milestones and potential. *NPG Asia Mater.* **2019**, *11*, No. 10.

(7) Kapat, K.; Shubhra, Q. T. H.; Zhou, M.; Leeuwenburgh, S. Piezoelectric Nano-Biomaterials for Biomedicine and Tissue Regeneration. *Adv. Funct. Mater.* **2020**, *30*, No. 1909045.
(8) Sun, Y.; Zeng, K. Y.; Li, T. Piezo-/ferroelectric phenomena in biomaterials: A brief review of recent progress and perspectives. *Sci. China: Phys., Mech. Astron.* **2020**, *63*, No. 278701.
(9) Yuan, H.; Han, P.; Tao, K.; Liu, S.; Gazit, E.; Yang, R. Piezoelectric Peptide and Metabolite Materials. *Research* **2019**, *2019*, 1−13.
(10) Lee, B. Y.; Zhang, J.; Zueger, C.; Chung, W. J.; Yoo, S. Y.; Wang, E.; Meyer, J.; Ramesh, R.; Lee, S. W. Virus-based piezoelectric energy generation. *Nat. Nanotechnol.* **2012**, *7*, 351−356.
(11) Kholkin, A.; Amdursky, N.; Bdikin, I.; Gazit, E.; Rosenman, G. Strong Piezoelectricity in Bioinspired Peptide Nanotubes. *ACS Nano* **2010**, *4*, 610−614.
(12) Lee, J.-H.; Heo, K.; Schulz-Schönhagen, K.; Lee, J. H.; Desai, M. S.; Jin, H.-E.; Lee, S.-W. Diphenylalanine Peptide Nanotube Energy Harvesters. *ACS Nano* **2018**, *12*, 8138−8144.
(13) Nguyen, V.; Zhu, R.; Jenkins, K.; Yang, R. Self-assembly of diphenylalanine peptide with controlled polarization for power generation. *Nat. Commun.* **2016**, *7*, No. 13566.
(14) Ryan, K.; Beirne, J.; Redmond, G.; Kilpatrick, J. I.; Guyonnet, J.; Buchete, N.-V.; Kholkin, A. L.; Rodriguez, B. J. Nanoscale Piezoelectric Properties of Self-Assembled Fmoc−FF Peptide Fibrous Networks. *ACS Appl. Mater. Interface* **2015**, *7*, 12702−12707.
(15) Ico, G.; Myung, A.; Kim, B. S.; Myung, N. V.; Nam, J. Transformative piezoelectric enhancement of P(VDF-TrFE) synergistically driven by nanoscale dimensional reduction and thermal treatment. *Nanoscale* **2018**, *10*, 2894−2901.
(16) Ghadiri, M. R.; Granja, J. R.; Milligan, R. A.; McRee, D. E.; Khazanovich, N. Self-assembling organic nanotubes based on a cyclic peptide architecture. *Nature* **1993**, *366*, 324−327.
(17) Seebach, D.; Beck, A. K.; Bierbaum, D. J. The world of β- and γ-peptides comprised of homologated proteinogenic amino acids and other components. *Chem. Biodiversity* **2004**, *1*, 1111−1239.
(18) Amorín, M.; Castedo, L.; Granja, J. R. New cyclic peptide assemblies with hydrophobic cavities: the structural and thermodynamic basis of a new class of peptide nanotubes. *J. Am. Chem. Soc.* **2003**, *125*, 2844−2845.
(19) Brea, R. J.; Reiriz, C.; Granja, J. R. Towards functional bionanomaterials based on self-assembling cyclic peptide nanotubes. *Chem. Soc. Rev.* **2010**, *39*, 1448−1456.
(20) Rodríguez-Vázquez, N.; Amorin, M.; Granja, J. R. Recent advances in controlling the internal and external properties of self-assembling cyclic peptide nanotubes and dimers. *Org. Biomol. Chem.* **2017**, *15*, 4490−4505.
(21) Hsieh, W. H.; Liaw, J. Applications of cyclic peptide nanotubes (cPNTs). *J. Food Drug Anal.* **2019**, *27*, 32−47.
(22) Chapman, R.; Danial, M.; Koh, M. L.; Jolliffe, K. A.; Perrier, S. Design and properties of functional nanotubes from the self-assembly of cyclic peptide templates. *Chem. Soc. Rev.* **2012**, *41*, 6023−6041.
(23) Kamano, Y.; Tabata, Y.; Uji, H.; Kimura, S. Chiral and random arrangements of flavin chromophores along cyclic peptide nanotubes on gold influencing differently on surface potential and piezoelectricity. *RSC Adv.* **2019**, *9*, 3618−3624.
(24) Tabata, Y.; Kamano, Y.; Uji, H.; Imai, T.; Kimura, S. Electronic Properties of Cyclic β-Peptide Nanotube Bundles Reflecting Structural Arrangement. *Chem. Lett.* **2019**, *48*, 322−324.
(25) Tabata, Y.; Mitani, S.; Uji, H.; Imai, T.; Kimura, S. The effect of macrodipole orientation on the piezoelectric response of cyclic β-peptide nanotube bundles on gold substrates. *Polym. J.* **2019**, *51*, 601−609.
(26) Clark, T. D.; Buehler, L. K.; Ghadiri, M. R. Self-Assembling Cyclic β^3-Peptide Nanotubes as Artificial Transmembrane Ion Channels. *J. Am. Chem. Soc.* **1998**, *120*, 651−656.
(27) Kimura, S. Molecular dipole engineering: new aspects of molecular dipoles in molecular architecture and their functions. *Org. Biomol. Chem.* **2008**, *6*, 1143−1148.
(28) Ishihara, Y.; Kimura, S. Four-peptide-nanotube bundle formation by self-assembling of cyclic tetra-β-peptide using G-quartet motif. *Biopolymers* **2013**, *100*, 141−147.
(29) Ishihara, Y.; Kimura, S. Peptide nanotube composed of cyclic tetra-β-peptide having polydiacetylene. *Biopolymers* **2012**, *98*, 155−160.
(30) Reiriz, Cs.; Brea, R. J.; Arranz, Ro.; Carrascosa, J. L.; Garibotti, A.; Manning, B.; Valpuesta, J. M.; Eritja, Rn.; Castedo, L.; Granja, J. R. α,γ-Peptide Nanotube Templating of One-Dimensional Parallel Fullerene Arrangements. *J. Am. Chem. Soc.* **2009**, *131*, 11335−11337.
(31) Tabata, Y.; Kamano, Y.; Kimura, S.; Uji, H. Engineering pH-responsive switching of donor−π−acceptor chromophore alignments along a peptide nanotube scaffold. *RSC Adv.* **2020**, *10*, 3588−3592.
(32) Ohmura, H.; Tabata, Y.; Kimura, S.; Uji, H. Piezoelectric properties reflecting nanostructures of tetrathiafulvalene and chloranil complexes using cyclic peptide nanotube scaffolds. *Pept. Sci.* **2020**, *113*, No. e24192.
(33) Hol, W. G.; van Duijnen, P. T.; Berendsen, H. J. The α-helix dipole and the properties of proteins. *Nature* **1978**, *273*, 443−446.
(34) Hol, W. G. The role of the α-helix dipole in protein function and structure. *Prog. Biophys. Mol. Biol.* **1985**, *45*, 149−195.
(35) Otoda, K.; Kitagawa, Y.; Kimura, S.; Imanishi, Y. Chain length dependent transition of 3_{10}- to α-helix of Boc-(Ala-Aib)n-OMe. *Biopolymers* **1993**, *33*, 1337−1345.
(36) Kai, M.; Takeda, K.; Morita, T.; Kimura, S. Distance dependence of long-range electron transfer through helical peptides. *J. Pept. Sci.* **2008**, *14*, 192−202.
(37) Toniolo, C.; Polese, A.; Formaggio, F.; Crisma, M.; Kamphuis, J. Circular Dichroism Spectrum of a Peptide 3_{10}-Helix. *J. Am. Chem. Soc.* **1996**, *118*, 2744−2745.
(38) Kennedy, D. F.; Crisma, M.; Toniolo, C.; Chapman, D. Studies of peptides forming 3_{10}- and α-helices and β-bend ribbon structures in organic solution and in model biomembranes by Fourier transform infrared spectroscopy. *Biochemistry* **1991**, *30*, 6541−6548.
(39) Matthews, J. L.; Gademann, K.; Jaun, B.; Seebach, D. Linear and cyclic β^3-oligopeptides with functionalised side-chains (-CH_2OBn, -CO_2Bn, -$CH_2CH_2CO_2Bn$) derived from serine and from aspartic and glutamic acid. *J. Chem. Soc., Perkin Trans. 1* **1998**, *8*, 3331−3340.
(40) Uji, H.; Kim, H.; Imai, T.; Mitani, S.; Sugiyama, J.; Kimura, S. Electronic properties of tetrathiafulvalene-modified cyclic-β-peptide nanotube. *Biopolymers* **2016**, *106*, 275−282.
(41) Miller, K. J. Calculation of the Molecular Polarizability Tensor. *J. Am. Chem. Soc.* **1990**, *112*, 8543−8551.
(42) Fujimura, F.; Hirata, T.; Morita, T.; Kimura, S.; Horikawa, Y.; Sugiyama, J. Columnar Assembly of Cyclic β-Amino Acid Functionalized with Pyranose Rings. *Biomacromolecules* **2006**, *7*, 2394−2400.
(43) Majdoub, M. S.; Sharma, P.; Cagin, T. Enhanced size-dependent piezoelectricity and elasticity in nanostructures due to the flexoelectric effect. *Phys. Rev. B* **2008**, *77*, No. 125424.
(44) Zhang, J.; Wang, C. Y.; Adhikari, S. Surface effect on the buckling of piezoelectric nanofilms. *J. Phys. D: Appl. Phys.* **2012**, *45*, No. 285301.
(45) Görbitz, C. H. The structure of nanotubes formed by diphenylalanine, the core recognition motif of Alzheimer's β-amyloid polypeptide. *Chem. Commun.* **2006**, 2332−2334.
(46) Silva, R. F.; Araujo, D. R.; Silva, E. R.; Ando, R. A.; Alves, W. A. L-diphenylalanine microtubes as a potential drug-delivery system: characterization, release kinetics, and cytotoxicity. *Langmuir* **2013**, *29*, 10205−10212.
(47) Fujimura, F.; Fukuda, M.; Sugiyama, J.; Morita, T.; Kimura, S. Parallel assembly of dipolar columns composed of a stacked cyclic tri-β-peptide. *Org. Biomol. Chem.* **2006**, *4*, 1896−1901.

https://doi.org/10.1021/acs.biomac.1c00213
Biomacromolecules 2021, 22, 2815−2821